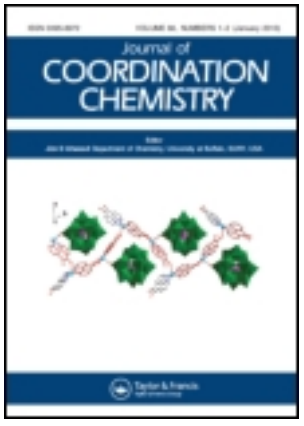

Journal of Coordination Chemistry
Publication details, including instructions for authors and subscription information:
http://www.tandfonline.com/loi/gcoo20

Ruthenium(II) complexes of pyrrol-azo ligands: cytotoxicity, interaction with calf thymus DNA and bovine serum albumin

Hena Paul [a], Titas Mukherjee [a], Manjira Mukherjee [a], Tapan K. Mondal [b], Anuradha Moirangthem [c], Anupam Basu [c], Ennio Zangrando [d] & Pabitra Chattopadhyay [a]

[a] Department of Chemistry, Burdwan University, Golapbag, Burdwan, India

[b] Department of Chemistry, Jadavpur University, Jadavpur, India

[c] Department of Zoology, Burdwan University, Golapbag, Burdwan, India

[d] Department of Chemical and Pharmaceutical Sciences, University of Trieste, Trieste, Italy

Accepted author version posted online: 14 Jun 2013.Published online: 16 Jul 2013.

To cite this article: Hena Paul, Titas Mukherjee, Manjira Mukherjee, Tapan K. Mondal, Anuradha Moirangthem, Anupam Basu, Ennio Zangrando & Pabitra Chattopadhyay (2013) Ruthenium(II) complexes of pyrrol-azo ligands: cytotoxicity, interaction with calf thymus DNA and bovine serum albumin, Journal of Coordination Chemistry, 66:15, 2747-2764, DOI: 10.1080/00958972.2013.814048

To link to this article: http://dx.doi.org/10.1080/00958972.2013.814048

Journal of Coordination Chemistry, 2013
Vol. 66, No. 15, 2747–2764, http://dx.doi.org/10.1080/00958972.2013.814048

Ruthenium(II) complexes of pyrrol-azo ligands: cytotoxicity, interaction with calf thymus DNA and bovine serum albumin

HENA PAUL†, TITAS MUKHERJEE†, MANJIRA MUKHERJEE†, TAPAN K. MONDAL‡, ANURADHA MOIRANGTHEM§, ANUPAM BASU§, ENNIO ZANGRANDO¶ and PABITRA CHATTOPADHYAY*†

†Department of Chemistry, Burdwan University, Golapbag, Burdwan, India
‡Department of Chemistry, Jadavpur University, Jadavpur, India
§Department of Zoology, Burdwan University, Golapbag, Burdwan, India
¶Department of Chemical and Pharmaceutical Sciences, University of Trieste, Trieste, Italy

(*Received 2 February 2013; in final form 29 April 2013*)

Two ruthenium(II) complexes of newly designed pyrrol-azo ligands(L) and bipyridine(bpy) formulated as $[Ru(L)(bpy)_2]ClO_4$, where HL^1 = *(4-chloro-phenyl)-(1H-pyrrol-2-yl)-diazene* (**1**) complex **1** and HL^2 = *(4-nitro-phenyl)-(1H-pyrrol-2-yl)-diazene* for **2**, were isolated in pure form. The complexes were characterized by physicochemical and spectroscopic methods. The electrochemical behavior of the complexes showed the Ru(III)/Ru(II) couple at different potentials with *quasi*-reversible voltammograms. The study of cytotoxicity effects of **1** and **2** on human breast cancer cells (MCF 7, MDA-MB 231) and cervical cancer cell (HeLa) taking Cisplatin as a positive reference showed that **1** exhibited higher cytotoxicity against cancer cell lines than **2**, but less activity than Cisplatin. The interaction of **1** with calf thymus DNA (CT-DNA) using absorption, emission spectral studies, viscosity-measurement, and electrochemical techniques has been used to determine the binding constant K_b and the linear Stern–Volmer quenching constant K_{SV}. The results indicate that **1** strongly interacts with CT-DNA in groove binding mode. The interaction of bovine serum albumin (BSA) with **1** was also investigated with the help of spectroscopic tools. Absorption spectroscopy proved the formation of a BSA-$[Ru(L^1)(bpy)_2]ClO_4$ complex.

Keywords: Ruthenium(II) complex; Phenylazopyrrole; Cytotoxicity; DNA Interaction

1. Introduction

Aryl- and heteroaryl-azopyrroles have been used extensively in the textile, fiber, leather, paint, and printing industries due to their ability to absorb visible light, and for their easy synthesis [1]. These ligands are interesting mainly because of presence of the azo group (–N=N–) which can stabilize ruthenium in lower oxidation states due to its strong π-acidic character. Such complexes are useful in metal-assisted organic transformations, and as metallochromic indicators and also show photochromic behavior [2–6]. Azophenyl complexes have been extensively used as catalysts for transfer hydrogenation of ketones

*Corresponding author. Email: pabitracc@yahoo.com

[7, 8]. Among the different metals catalyzing reaction, ruthenium-based systems are effective [9–11].

Variable oxidation states of ruthenium complexes containing nitrogen heterocycles are useful as building blocks for supramolecular assemblies, photophysical properties, directional electron and energy transfer, DNA intercalation, and potential antitumor activities [12–15]. A wide range of ruthenium compounds have been used as potential anticancer drugs [16–20]. The study of their interaction with proteins, DNA, and lipids has received considerable attention because of the spectroscopic and redox properties of ruthenium(II) complexes with heterocyclic N-donors, the higher coordination number of ruthenium compared with platinum providing additional coordination sites, and due to the possible application in biochemistry and clinical diagnosis [21–23]. Bovine serum albumin has a wide range of physiological functions involving binding, transport, and delivery of fatty acids, porphyrins, bilirubin, steroids, etc. It has specific binding sites for metals and pharmaceutical dyes [24].

Considering the above facts and our ongoing interest towards the study of interaction of metal chelates with CT-DNA [25–28] and BSA [29], herein we report synthesis and characterization, cytotoxicity of **1** and **2** towards human breast cancer cells (MCF 7, MDA-MB 231) and cervical cancer cell (HeLa), DNA binding, and protein binding study of **1**. The redox behavior of these complexes in acetonitrile by cyclic voltammetry has also been studied. Binding of **1** and **2** with bovine serum albumin (BSA) was studied by absorption and fluorescence spectroscopy.

2. Experimental

2.1. *Materials and physical measurements*

All chemicals and reagents were obtained from commercial sources and used as received. Solvents were distilled from an appropriate drying agent. $RuCl_3 \cdot 3H_2O$ (Aldrich) was used without purification. $[Ru^{II}Cl_2(bpy)_2] \cdot 2H_2O$ was synthesized according to the literature method [30]. Tetra-*n*-butylammonium perchlorate (TBAP) was prepared by addition of sodium perchlorate (taking the usual precaution of handling perchlorate salts !) to a hot solution of tetra-*n*-butylammoniumbromide (Aldrich).

The C, H, and N elemental analyses were performed on a Perkin-Elmer model 2400 elemental analyzer and ruthenium analyses were carried out by a Varian atomic absorption spectrophotometer (AAS) model-AA55B, GTA using a graphite furnace. Electronic absorption spectra were recorded on a JASCO UV–vis/NIR spectrophotometer model V-570 from 1100–200 nm. IR spectra (KBr disks, 4000–300 cm^{-1}) were recorded using a Perkin-Elmer FTIR model RX1 spectrometer. ^1H NMR spectra were recorded on a Bruker AC300 spectrometer using TMS as internal standard in $CDCl_3$. Room temperature magnetic susceptibility measurements were performed with a vibrating sample magnetometer PAR 155 model. Molar conductances (Λ_M) were measured in a Systronics conductivity meter (model 304) in acetonitrile with $\sim 10^{-3}$ M L^{-1}. The measurement of pH was done with a Systronics digital pH meter (Model 335). Electrochemical measurements were recorded on a CH-Instrument electrochemical system (Model 620D) using Pt-wire and Ag/AgCl as working and reference electrodes, respectively, taking TBAP as supporting electrolyte. All measurements were made at 298 K with 10^{-3}–10^{-4} M complex in acetonitrile purged with dry nitrogen for 3–4 min in order to remove dissolved oxygen.

2.2. *Synthesis of compounds*

2.2.1. Preparation of HL^1 and HL^2. Ligands were synthesized following the common procedure of coupling pyrrole with the corresponding diazotized *para*-substituted aniline (scheme 1). The procedure for preparation of *(4-chloro-phenyl)-(1H-pyrrol-2-yl)-diazene* (HL^1) is described in detail; the other ligand was obtained as solid product in the same way.

(4-Chloro-phenyl)-(1H-pyrrol-2-yl)-diazene (HL^1): Initially a diazotized solution of 4-chloro-aniline (2.55 g, 20.0 mM) was prepared using ice-cold 2.0 mL conc. HCl and aqueous $NaNO_2$ (0.56 g). Then the diazotized solution was added dropwise to the solution of pyrrole (1.35 g, 20.9 mM) in aqueous Na_2CO_3 solution at 0–5 °C with continuous stirring. The pH of the reaction mixture was maintained at 7–9 by adding Na_2CO_3 solution dropwise if necessary. The red compound that precipitated was filtered (scheme 1). Finally the compound was purified through recrystallization from a mixture of dichloromethane and *n*-hexane (1 : 1). The reddish-brown single crystals of HL^1 suitable for X-ray crystallography were obtained from a hexane-toluene mixture of the compound on slow evaporation at room temperature.

$C_{10}H_8ClN_3$: Anal. Found: C, 58.39; H, 3.89; N, 20.44; Calcd: C, 58.41; H, 3.92; N, 20.43. m.p. 72 ± 1 °C. IR (KBr, cm^{-1}): ν_{N-H}, 3453, $\nu_{N=N}$, 1425. ^1H NMR (δ, ppm; J, cps; in $CDCl_3$): 9.75 (s, 1H); 7.351 (d, 1H, J = 5.1); 6.753 (d, 2H, J = 7.3); 6.624 (d, 2H, J = 8.53); 6.326 (m, 1H); 6.173 (s, 1H). ESI-MS (m/z): $[M+H]^+$, 206.34. Yield: 85%.

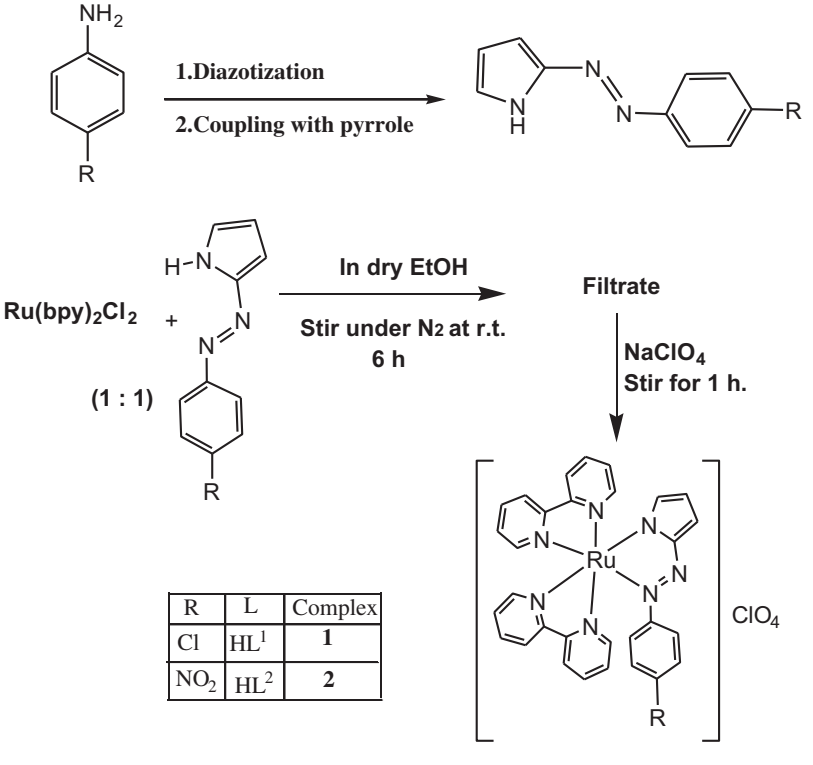

R	L	Complex
Cl	HL^1	**1**
NO_2	HL^2	**2**

Scheme 1. Synthetic procedure of organic moieties (HL) and **1** and **2**.

(4-nitro-phenyl)-(1H-pyrrol-2-yl)-diazene (HL^2): HL^2 was prepared taking *4*-nitro-aniline (2.76 g, 20.0 mM) instead of *para*-chloro-aniline following similar method.

$C_{10}H_8N_4O_2$: Anal. Found: C, 55.47; H, 3.70; N, 25.74; Calcd: C, 55.55; H, 3.73; N, 25.91. m.p. 111 ± 1 °C. IR (KBr, cm^{-1}): ν_{N-H}, 3450, $\nu_{N=N}$, 1420. ^1H NMR (δ, ppm; J, cps; in $CDCl_3$): 9.77 (s, 1H); 7.472 (d, 1H, J = 5.4); 7.324 (d, 2H, J = 5.5); 7.063 (d, 2H, J = 7.45); 6.532 (m, 1H); 6.410 (s, 1H). ESI-MS: $[M+H]^+$, m/z, 217.15; Yield: 80%.

2.2.2. Preparation of ruthenium(II) complexes (1 and 2). To an ethanolic solution of the respective organic moiety (0.205 g, 1.0 mM of HL^1 or 0.216 g, 1.0 mM of HL^2), a solution of $[RuCl_2(bpy)_2]$ (0.484 g, 1.0 mM) in dry EtOH (20 mL) previously purged with N_2 was added dropwise and the resulting solution was stirred for ~6 h under N_2. The solvent volume of the resulting solution was reduced to one third of the total and a water solution of $NaClO_4$ (0.140 g, 1 mM) was added dropwise with stirring. The resulting mixture was stirred for ~2 h and then a red solid was obtained by filtration. The product was dissolved in minimum dichloromethane and pure ruthenium complex was obtained by chromatographic separation over a silica gel column prepared in dichloromethane (scheme 1).

$[Ru(L^1)(bpy)_2]ClO_4$ (**1**): $C_{30}H_{23}Cl_2N_7O_4Ru$: Anal. Found: C, 50.11; H, 3.16; N, 13.75; Ru, 14.17; Calcd: C, 50.22; H, 3.23; N, 13.66; Ru, 14.09. IR (KBr, cm^{-1}): $\nu_{N=N}$, 1385; $\nu_{(ClO4-)}$, 1088 and 624. Conductance Λ_o (Ω^{-1} cm^2 M^{-1}) in methanol: 91. ^1H NMR (δ, ppm; J, cps; in $CDCl_3$): 8.372 (t, 2H); 8.255 (d, 1H, J = 5); 8.177 (d, 1H, J = 8.1); 8.115 (d, 1H, J = 8); 7.905–7.832 (m, 3H); 7.719 (m, 2H); 7.584 (d, 1H, J = 5.3); 7.410 (d, 1H, J = 5.25); 7.293–7.236 (m, 5H); 6.863 (d, 2H, J = 8.75); 6.759 (d, 2H, J = 8.75); 6.439 (q, 1H); 6.281 (s, 1H). ESI-MS (m/z): $[Ru(L^1)(bpy)_2]$ + H^+, 618.2 (100% abundance); $[Ru(L^1)(bpy)_2]ClO_4 + K^+$, 756 (10% abundance). Yield: 70–72%.

$[Ru(L^2)(bpy)_2]ClO_4$ (**2**): $C_{30}H_{23}ClN_8O_6Ru$: Anal. Found: C, 49.45; H, 3.15; N, 15.38; Ru, 13.82; Calcd: C, 49.49; H, 3.18; N, 15.39; Ru, 13.88. IR (KBr cm^{-1}): $\nu_{N=N}$, 1384; $\nu_{(ClO4-)}$, 1091 and 626. Conductance Λ_o (Ω^{-1} cm^2 M^{-1}) in methanol: 102. ^1H NMR (δ, ppm; J, cps; in $CDCl_3$): 8.453 (m, 2H); 8.287 (d, 1H, J = 5); 8.201 (m, 2H); 8.016-7.959 (m, 3H); 7.927 (m, 1H); 7.866-7.830 (m, 4H); 7.677 (d, 1H, J = 4.5); 7.501 (d, 1H, J = 5.5); 7.461 (d, 1H, J = 4.5); 7.389-7.354 (m, 3H); 7.102 (d, 2H, J = 9); 6.640 (q, 1H); 6.507 (s, 1H). ESI-MS (m/z): $[Ru(L^2)(bpy)_2]$ + H^+, 632.2 (60% abundance). Yield: 70–72%.

2.3. *X-ray crystal structure analysis*

Single crystals suitable for X-ray diffraction study of HL^1 were grown by slow evaporation of a methanolic solution at ambient temperature. Diffraction data collection of L^1H was carried out at 150(2) on an Oxford Diffraction Xcalibur CCD system using Mo Kα radiation (λ = 0.71073 Å). Cell refinement, indexing, and scaling of the data-set were performed using CrysAlis [31], Denzo, and Scalepack [32]. The structure was solved by direct methods and refined by full-matrix least-squares based on F^2 with all observed reflections [33]. Hydrogens were fixed at geometrical positions. All calculations were performed using the WinGX system, Ver 1.80.05 [34]. Details of the crystal data and structure refinement are given in table 1.

Table 1. Crystal data and details of refinement for HL^1.

Empirical formula	$C_{10}H_8N_3Cl$
Formula weight	205.64
Crystal system	Triclinic
Space group	$P\bar{1}$
a (Å)	7.6867(4)
b (Å)	9.9521(6)
c (Å)	12.7722(6)
α (°)	82.262(4)
β (°)	89.479(4)
γ (°)	78.194(5)
Volume (Å^3)	947.51(9)
ρ_{calc} [g/cm^3]	1.442
Z	4
F (000)	424
θ range (°)	3.07–25.00
μ (Mo K_α) (mm^{-1})	0.362
Collected/unique reflections	20,544/6672
Reflections $I > 2\sigma(I)$	3313
Parameters	253
Goodness-of-fit	0.848
Final R indices [$I > 2\sigma(I)$]	$R1 = 0.0330$, $wR2 = 0.0592$
R indices (all data)	$R1 = 0.0614$, $wR2 = 0.0630$
Residuals (e.Å^{-3})	0.432, −0.453

2.4. *DFT calculation*

Full geometry optimization was carried out using density functional theory at the B3LYP level for **1** and **2** [35]. All elements except ruthenium were assigned the 6–31G(d) basis set. The SDD basis set with effective core potential was employed for ruthenium [36]. The vibrational frequency calculations were performed to ensure that the optimized geometries represent local minima and there are only positive eigenvalues. All calculations were performed with the Gaussian03 program package. Vertical electronic excitations based on B3LYP optimized geometry were computed using the time-dependent density functional theory (TD-DFT) formalism [37] in acetonitrile using conductor-like polarizable continuum model (CPCM). GaussSum [38] was used to calculate the fractional contributions of various groups to each molecular orbital.

2.5. *Cytotoxicity assay*

For this study, human breast cancer epithelial cell (MCF 7) and cervical cancer cell (HeLa) were cultured in DMEM medium supplemented with 10% fetal bovine serum and 1% penicillin-streptomycin at 37 °C in a humidified atmosphere containing 5% CO_2. The mesenchymal type of breast cancer cell (MDA-MB 231) was cultured in L-15 medium supplemented with 10% fetal bovine serum and 1% penicillin–streptomycin at 37 °C in a humidified atmosphere without CO_2.

The 3-(4,5-dimethylthiazol-2yl)-2,5-diphenyltetrazoliumbromide (MTT) was used to assess the cytotoxic effect of **1** and **2**. Human cancer cells (MCF7, MDA MB 231, and HeLa) were seeded in 24-well culture plate with a seeding density of 10×10^4 cells per well in 500.0 µl of complete medium. Cells were treated with different concentrations of the ruthenium complexes (0.2–60.0 µg/ml) for 24 h along with controlled experiments with standard Cisplatin for comparison. At the end of the treatment period, 50.0 µl of MTT

(5.0 mg/ml in PBS) was added in each well and incubated for 3 h at 37 °C. Media containing MTT was removed and the formazon was dissolved with DMSO. Absorbance was measured spectrophotometrically at 590 nm.

2.6. *DNA binding experiments*

The *tris*–HCl buffer solution (pH 7.4), used in all the experiments involving CT-DNA, was prepared using deionized and sonicated HPLC grade water (Merck). The CT-DNA was sufficiently free from protein, with the ratio of UV absorbance of DNA in *tris*–HCl solution at 260 and 280 nm (A260/A280) of ca. 1.9 [39]. The concentration of DNA was determined with its extinction coefficient ε of 6600 L M^{-1} cm^{-1} at 260 nm [40]. The stock solution of DNA was always stored at 4 °C and used within four days. Concentrated stock solution of complex was prepared by dissolving **1** in DMSO and suitably diluting with *tris*–HCl buffer to the concentration required for all the experiments. Absorption spectral titration was performed by keeping constant the concentration of **1** while varying the CT-DNA concentration. To eliminate the absorbance of DNA itself, an equal solution of CT-DNA was added to the ruthenium(II) complex solution and to the reference. In the fluorescence displacement experiment with ethidium bromide (EB), 5.0 μL of EB solution (1.0 mM L^{-1}) in *tris*–HCl was added to 1.0 mL of DNA solution at saturated binding levels [41], and stored in the dark for 2.0 h. Solution of **1** was titrated into the DNA/EB mixture and then diluted in *tris*–HCl buffer to 5.0 mL, making solutions with varied mole ratio of the metal complex to CT-DNA. Prior to measurements, the mixture was shaken and incubated at room temperature for 30 min. The fluorescence spectra of EB bound to DNA were obtained at an emission wavelength of 584 nm.

To adjudge the binding mode (groove/intercalative) of **1** with DNA, the well-known method using Ostwald's viscometer was used. Titrations were performed by introducing **1** (0.5–3.5 μM) into a CT-DNA solution (5.0 μM) present in the viscometer. The viscosity values of the solutions were calculated from the observed flow time of CT-DNA-containing solution corrected from the flow time of buffer alone (t_0), $\eta = t - t_0$. The calculated data were used to plot the $(\eta/\eta_0)^{1/3}$ *versus* the ratio of the concentration of **1** and CT-DNA, where η is the viscosity of CT-DNA in the presence of the compound and η_0 is the viscosity of CT-DNA alone.

2.7. *Protein (bovine serum albumin) binding experiments*

Samples for spectroscopic measurements were prepared by dissolving bovine serum albumin in water and administering the appropriate concentration of **1**. The samples were carefully degassed using pure nitrogen for 15 min. Quartz cells with high vacuum Teflon stopcocks were used for degassing.

2.8. *Cyclic voltammetry (CV) experiments*

Voltammetric measurements were carried out in a one-compartment cell using a Pt disk (area, 0.023 cm^2) working electrode, a Pt flag counter electrode, and a Ag/AgCl reference electrode. Typical CV curves for 0.1 mM **1** and **2** in *tris*-buffer in absence and presence of CT-DNA were carried out.

3. Results and discussion

3.1. *Synthesis and characterization*

HL^1 and HL^2 were prepared by coupling pyrrole with the diazonium ion obtained from the corresponding *para*-substituted aniline. These organic moieties are bidentate NN donors, interesting due to the presence of hard donor azo-N and borderline base pyrrolic-N centers. The ligand has been characterized by spectroscopic tools and X-ray diffraction studies. Complexes **1** and **2** were obtained in good yield from reaction of $[RuCl_2(bpy)_2]$ with equimolar amount of HL^1 or HL^2 in refluxing dry ethanol under dinitrogen, followed by addition of aqueous solution of sodium perchlorate to the resulting reaction mixture after cooling (*viz*. scheme 1).

Complexes **1** and **2** are soluble in DCM, acetonitrile, methanol, and DMF. Microanalytical data confirm the formulation of **1** and **2**. Both **1** and **2** are 1 : 1 electrolytes as determined by the observed conductivity (Λ_o) of 91–102 mho $cm^2 M^{-1}$ in methanol, and the magnetic moment studies demonstrate that the complexes are diamagnetic in nature.

3.2. *Structure of HL^1*

Single crystals of HL^1 were obtained from a hexane–toluene solvent mixture of the compound on slow evaporation at room temperature. The crystal structure of the ligand is shown in figure S1 together with the atom labeling scheme for all non-H atoms, and a selection of bond lengths and angles appear in table 2.

The crystallographic independent unit comprises molecules A and B, which are comparable with respect to bond distances and angles, as indicated in table 2 where values of A and B agree within their esd's. The molecules are arranged about a pseudo inversion center, but oriented so that their mean planes form a dihedral angle of 53.1°. This disposition allows the double H-bond interactions N–H…N of 3.012 and 3.074 Å (see figure S1). Both molecules present coplanar atoms, indicating an electron delocalization inside each

Table 2. Selected bond lengths (Å) and angles (°) of the two independent molecules of HL^1.

Molecule A		Molecule B	
C(1a)–N(7a)	1.429(2)	C(1)–N(7)	1.435(2)
N(7a)–N(8a)	1.280(2)	N(7)–N(8)	1.281(2)
N(8a)–C(9a)	1.374(2)	N(8)–C(9)	1.382(2)
C(9a)–N(10a)	1.384(2)	C(9)–N(10)	1.377(2)
C(9a)–C(13a)	1.387(3)	C(9)–C(13)	1.388(3)
N(10a)–C(11a)	1.362(2)	N(10)–C(11)	1.356(2)
C(2a)–C(1a)–N(7a)	124.08(19)	C(2)–C(1)–N(7)	125.51(17)
C(6a)–C(1a)–N(7a)	116.52(18)	C(6)–C(1)–N(7)	115.54(17)
N(8a)–N(7a)–C(1a)	113.81(16)	N(8)–N(7)–C(1)	113.61(16)
N(7a)–N(8a)–C(9a)	114.85(16)	N(7)–N(8)–C(9)	113.86(17)
N(10a)–C(9a)–N(8a)	126.01(18)	N(10)–C(9)–N(8)	126.60(18)
N(10a)–C(11a)–C(12a)	108.99(18)	N(10)–C(11)–C(12)	109.10(18)
C(11a)–C(12a)–C(13a)	107.42(18)	C(11)–C(12)–C(13)	107.27(17)
N(10a)–C(9a)–C(13a)	107.45(18)	N(10)–C(9)–C(13)	107.48(17)
N(8a)–C(9a)–C(13a)	126.53(19)	N(8)–C(9)–C(13)	125.92(18)
C(11a)–N(10a)–C(9a)	108.48(17)	C(11)–N(10)–C(9)	108.79(17)

molecule. The crystal packing shows A parallel aligned in a head-tail arrangement (being referred by a crystallographic center of symmetry) to form weak π–π interactions between the phenyl and pyrrole ring of the adjacent symmetry related molecule (and similarly do the molecules B, viz. figure S2).

3.3. *DFT computations: explanation of spectral and redox properties*

DFT calculation has been performed for **1** and **2**. The optimized structures of these molecules are developed using GAUSSIAN 03 (figure 1). The calculated bond angles and lengths for **1** and **2** are given in table S1. The orbital energies along with contributions from the ligands and metal are given in table S2 and figure S3, which depicts selected occupied and unoccupied frontier orbitals for **1**). The HOMO of **1** is constituted by 80% contribution from L, whereas to HOMO-2 bpy contributes 19% and the metal ion 75%. The LUMO-2 is composed of L by 74%. Thus, HOMO-2→LUMO is considered as major transition corresponding to Ru(dπ)→bpy(π*). The other transitions are HOMO→LUMO [Ru(dπ)/L(π)→bpy(π*), HOMO-1→LUMO [Ru(dπ)/L(π)→bpy(π*) and HOMO-2→LUMO + 1 [Ru(dπ)→bpy(π*)] that are intraligand and ligand-to-ligand charge transfer transitions. All these transitions are observed for **1**, and the calculated transitions are reported in table S3. Solvent polarity stabilizes occupied MOs more efficiently than unoccupied MOs. Thus, the energy separation (DE) between HOMO and LUMO increase on going from gas phase to MeCN solution.

Figure S4, depicts selected occupied and unoccupied frontier orbitals of **2**. The metal significantly contributes to the occupied MOs (76%, comparable to 75% of **1**). Bipyridine contributes 18% to HOMO-2 and 95% to LUMO in **2**. The orbital energies of **2** along with contributions from the ligands and metal are given in table S4 and the calculated transitions are in table 3. The intensity of these transitions has been assessed from oscillator strength (f). In MeCN, the longest wavelength band is calculated at >550 nm (f, 0.0067) for **1** followed by transitions at 502.3, 467.2, 448.9, and 395.4 nm along with a large number of transitions in the UV region (<400 nm). In **2**, the calculated transitions are 558.0 (f, 0.0435), 512.0 (f, 0.0894), 458.1 (f, 0.0872), and 444.5 (f, 0.0773) nm. The observed transitions are in agreement with the calculated ones for both complexes.

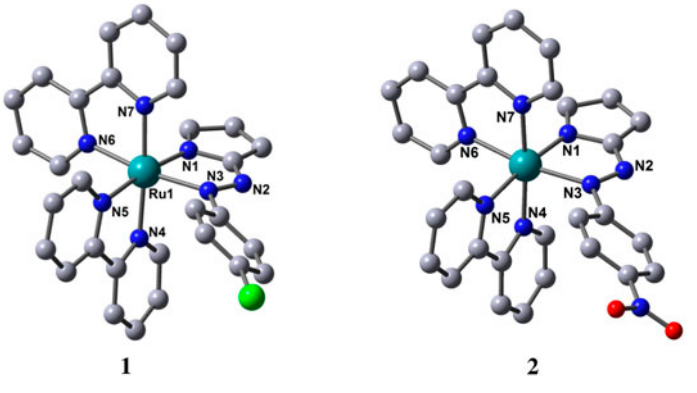

Figure 1. Optimized structure of **1** and **2** at DFT-B3LYP/6–31G(d) level of theory.

3.4. *Spectral properties*

IR spectra of the complexes are compared with the free ligands to confirm ligand coordination. The IR spectrum of HL^1 showed a band at ~3455 cm^{-1} for ν_{N-H}, which is absent in spectra of **1**, and that for L^2H at ~3210 cm^{-1} is also absent in spectra of **2** [42]. The $\nu_{N=N}$ in HL^1 is 1425 cm^{-1} and shifts to lower wavenumber in **1**, suggesting coordination. Similar result was obtained for **2**. Bands at 1380–1385 cm^{-1} are assigned to $\nu_{(N=N)}$ of coordinated azo (L^1/L^2) in the complexes [43]. Going from –N = N–($\sigma^2\pi^2$) to ($\sigma^2\pi^2$ π^{*1}), the bond order decreases from 2 to 1.5; therefore, the frequency of $\nu_{(N=N)}$ decreases significantly from free ligand (1420–1425 cm^{-1}). Here back-bonding from Ru(dπ) to azo(π^*) orbitals is expected to become unimportant upon azo anion radical formation. The complexes $[Ru(L)(bpy)_2]ClO_4$ show sharp absorptions at 1090 and 626 cm^{-1} assignable to $\nu_{(ClO4-)}$, which are absent for the organic moieties.

The ^1H NMR spectra of ligands and $[Ru(L)(bpy)_2]ClO_4$ were recorded in $CDCl_3$. The signals for L^1 and L^2 appeared in the spectra as usual in support of the proposed structural formulas. In the ^1H NMR spectra of the complexes, the protons appeared at higher δ values with respect to the free organic moieties. The NH-pyrrole signal is at δ = ~9.75 ppm, which is absent in ^1H NMR spectra of the complexes. Mass spectra of the complexes (figures S5 and 6) are also in support of these molecular structures.

Electronic absorption spectra of the complexes were recorded at room temperature using acetonitrile and data are reported in table 4. The spectra of the complexes exhibit the characteristic transitions at 295–297 nm and 375–378 nm corresponding to intramolecular $\pi\rightarrow\pi^*$ and $n\rightarrow\pi^*$ transitions, respectively. Bands at 489 and 493 nm in **1** and **2**, respectively, were observed due to the $d(Ru)\rightarrow\pi^*$(ligand) MLCT transitions.

3.5. *Electrochemical behavior*

The redox properties of **1** and **2** were examined by cyclic voltammetry using a Pt-disk working electrode, a Pt-wire auxiliary electrode, and Ag/AgCl electrode as reference in dry MeCN using $[n\text{-}Bu_4N]ClO_4$ (0.1 M) as the supporting electrolyte. Voltammetric data are given in table 4. Each complex exhibits a quasi-reversible Ru^{II}/Ru^{III} redox couple around a redox wave at ca. $E_{1/2}$ of 0.845 V (*versus* Ag/AgCl) for **1** and at ca. $E_{1/2}$ of

Table 3. Some selected vertical electronic excitations of **2**.

$E_{excitation}$ (eV)	$\lambda_{excitation}$ (nm)	Osc. strength (f)	Key transitions	Character	$\lambda_{expt.}$ (nm)
2.2219	558.0	0.0435	(86%)HOMO→LUMO	Ru(dπ)/L(π)→bpy(π*)	
2.4216	512.0	0.0894	(87%)HOMO-1→LUMO	Ru(dπ)/L(π)→bpy(π*)	495
2.7060	458.1	0.0872	(77%)HOMO-2→LUMO + 1	Ru(dπ)/bpy(π)→bpy(π*)	
2.7888	444.5	0.0773	(68%)HOMO-3→LUMO + 1	Ru(dπ)/bpy(π)→bpy(π*)	
3.0804	402.4	0.2219	(61%)HOMO-1→LUMO + 3	Ru(dπ)/L(π)→bpy(π*)	379
3.5166	357.6	0.1302	(69%)HOMO-3→LUMO + 4	Ru(dπ)/L(π)→bpy(π*)	
4.1865	296.2	0.0411	(47%)HOMO-6→LUMO + 2 (34%)HOMO-7→LUMO + 2	L(π)→L(π*)	299
4.3734	283.5	0.1145	(43%)HOMO-7→LUMO + 2 (27%)HOMO-6→LUMO + 2	L(π)→L(π*)	

Table 4. UV–vis spectral and electrochemical data[a].

Compd.	λ nm (ε) (ε, $dm^3\,mol^{-1}\,cm^{-1}$)	Electrochemical data $E_{1/2}$, ΔE (V) for Ru(II)/Ru(III)
1	489(2277), 375(3886), 297(4485)	0.845 (0.101)
2	495(2536), 379(3963), 299(4563)	1.11 (0.084)

[a]In acetonitrile.

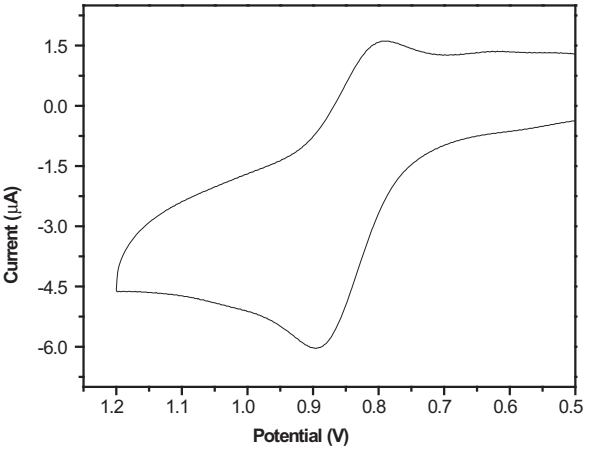

Figure 2. Cyclic voltammogram of **1** in MeCN (0.1 M n-Bu_4NClO_4) at 298 K, Ag/AgCl reference electrode, and scan rate 100 mV/s.

1.11 V (*versus* Ag/AgCl) for **2** at 25 °C (*viz*. figure 2). No cathodic response for $Ru^{II}\rightarrow Ru^{I}$ reduction was obtained for the complexes up to −1.50 V. The voltammetric parameters were studied in the scan rate interval 50–400 mV s^{-1}. The ratio between the cathodic peak current and the square root of the scan rate ($I_{pc}/v^{1/2}$) is approximately constant. The peak potential shows a small dependence on the scan rate. The ratio I_{pc} to I_{pa} is close to unity. From these data, it can be concluded that the redox couple is related to a quasi-reversible one-electron transfer controlled by diffusion.

3.6. *Cytotoxicity*

The cytotoxicities of **1** and **2** were tested on human cervical cancer HeLa cell line taking the Cisplatin as a positive reference. The activity is expressed as the concentration of the complexes required to inhibit the cellular survival fraction to 50% (LC_{50}). The results presented in table 5 indicate that **1** exhibits higher cytotoxicity against HeLa cell line and **2** is much less active than Cisplatin. The experiment with another cell lines shows that **1** is also the dose dependent inhibition of the proliferation of human breast cancer cells MCF 7 and MDA-MB 231. The LC_{50} value of **1** for HeLa, MCF 7, and MDA-MB 231 cells were 22, 22, and 20 μg/mL, respectively, whereas that of Cisplatin for MCF 7 and MDA-MB 231 were 50 and 56 μg/mL, respectively. This study clearly indicates that **1** is better than Cisplatin in terms of cytotoxicity. The activity of **1** over **2** may be caused by **1** being more

Table 5. Cytotoxicity (LC_{50}, μg/mL) of **1** and **2** (24 h).

Complex	HeLa	MCF 7	MDA MB 231
Cisplatin	42.6	50	56
1	22	22	20
2	75.4	Not significant	Not significant

lipophilic than **2**, facilitating the passive uptake of drug molecules across the lipidic cell membrane and hence enhancing the cytotoxicity [44]. However, both these ruthenium(II) complexes (**1** and **2**) possess better antitumor activity than earlier reports of cytotoxicity of octahedral ruthenium(II) complexes having two 2,2′-bipyridine moieties as coligands [45, 46].

3.7. *DNA binding experiments*

3.7.1. Electronic absorption titration. From the cytotoxic assay, **1** has very significant cytotoxic effect compared to **2** and even better than Cisplatin. As a result, the interaction of CT-DNA with **1** was examined.

The binding mode of **1** with calf thymus DNA was examined by electronic absorption titration with CT-DNA. As shown in figure 3, the spectra indicate a significant hyperchromism centered around 375 nm, suggesting a strong interaction between **1** and DNA. The spectral change might be interpreted as due to groove binding [47], since **1** contains azopyrrole, which could facilitate formation of van der Waals contacts or hydrogen bonds during interaction with DNA grooves. From these titration data, the intrinsic binding constant (K_b) of **1** with CT-DNA has been determined using the following equation (1) [48],

$$[\mathrm{DNA}]\ (\varepsilon_a - \varepsilon_f) = [\mathrm{DNA}]/(\varepsilon_b - \varepsilon_f) + 1/[k_b(\varepsilon_b - \varepsilon_f)] \quad (1)$$

where [DNA] represents the DNA concentration, ε_f and ε_b are the extinction coefficients for the free and fully bound **1**, respectively, and ε_a the complex extinction coefficient during each addition of DNA. The $[\mathrm{DNA}]/(\varepsilon_a - \varepsilon_f)$ plot against [DNA] gave a linear relationship (figure 4). The intrinsic binding constant (K_b) for **1** is calculated from the slope to intercept ratio ($K_b = 1.0 \times 10^5\ \mathrm{M}^{-1}$, $R = 0.\ 0.95469$ for five points). The value is in agreement with those of established groove binding rather than classical intercalation [49].

3.7.2. Ethidium bromide fluorescence displacement experiments. Ethidium bromide (EB) fluorescence displacement experiments were also performed to investigate the interaction mode of the complexes with CT-DNA. EB fluorescence intensity (at $\lambda_{ex} = 522$) will be enhanced in the presence of DNA because of its intercalation into the helix, and quenched by the addition of another molecule that displaces EB from DNA. Here, the fluorescence intensity of EB bound to DNA at 620 nm decreases by increasing the concentration of **1**, as shown in figure 5. EB fluorescence quenching due to release of some EB from the EB-DNA system is supportive to interaction of **1** with CT-DNA through groove binding. The

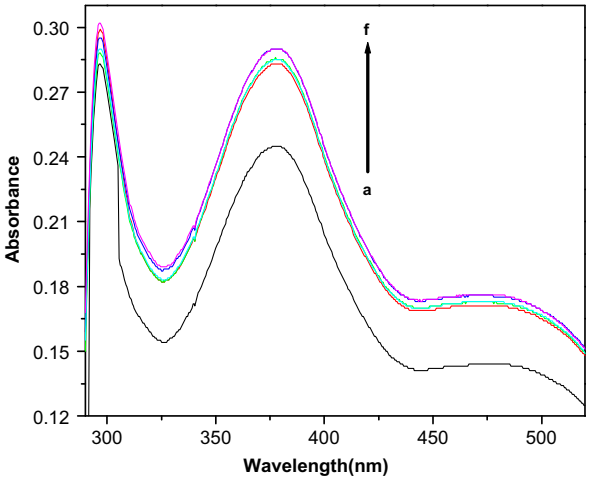

Figure 3. Electronic spectra of **1** through titration with CT-DNA in *tris*-HCl. The increase of DNA concentration is indicated by an arrow.

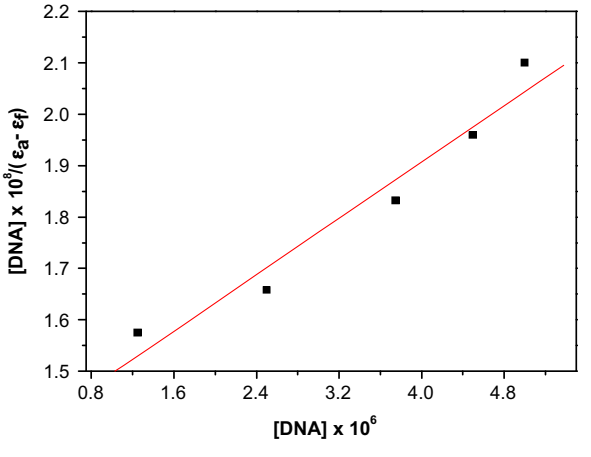

Figure 4. Plot of $[DNA]/(\varepsilon_a - \varepsilon_f)$ *vs.* [DNA] for titration of CT-DNA with **1** in *tris*-HCl buffer; binding constant $K_b = 1 \times 10^5\ M^{-1}$ ($R = 0.\ 0.95469$ for five points).

quenching trend of EB bound DNA by **1** is in agreement with the linear Stern–Volmer equation (2) [50]:

$$I_0/I = 1 + K_{SV}[\text{complex}] \quad (2)$$

where I_0 and I represent the fluorescence intensities in the absence and presence of quencher, respectively. K_{SV} is the linear Stern–Volmer quenching constant and [complex] the molar concentration of the quencher. From the slope of the regression line in the derived plot of I_0/I *versus* [complex] (figure 6), the K_{SV} value for the complex was determined as 1.125×10^4 for **1** ($R = 0.99023$ for five points), indicating strong affinity of **1** to CT-DNA.

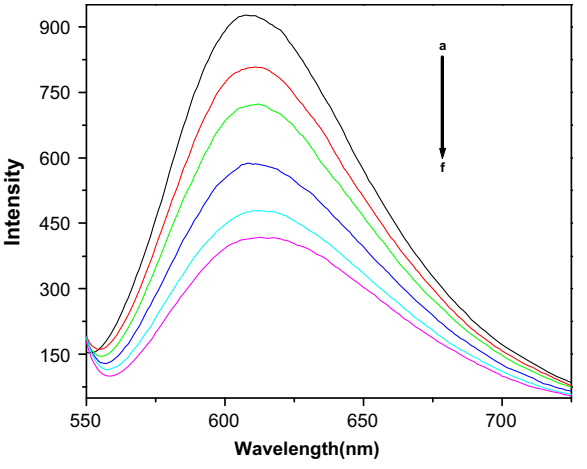

Figure 5. Emission spectra of CT-DNA-EB system in *tris*–HCl buffer based on titration of complex. $\lambda_{ex} = 522$ nm.

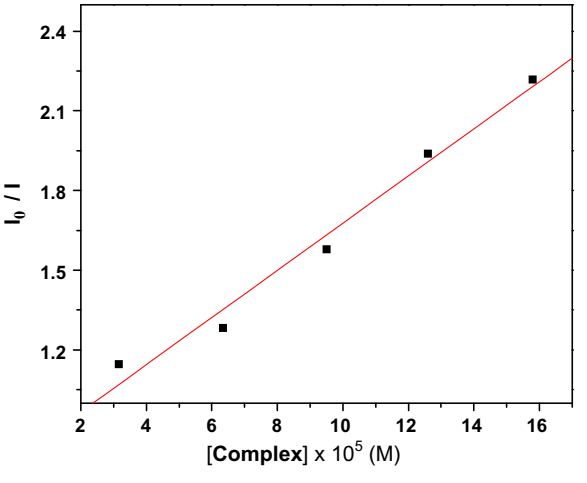

Figure 6. Plot of I_0/I *vs*. [complex] for titration of CT-DNA–EB system with **1** using spectrofluorimeter; linear Stern–Volmer quenching constant (K_{SV}) = 1.125×10^4 ($R = 0.99023$ for five points).

3.7.3. Viscosity. From spectroscopy, it was observed that **1** has a strong interaction with DNA. To further clarify the interactions between **1** and DNA, viscosity measurements were carried out. From this experiment there is almost no effect on the relative viscosity of the DNA solution, suggesting that the binding mode is groove binding, in support of the results obtained in the spectroscopic study. If **1** intercalated, increase of the relative viscosity of the DNA solution would be observed because intercalation leads to lengthening the DNA helix. Non-classical intercalation could bend (or kink) the DNA helix and reduce its effective length and, concomitantly, its viscosity [51, 52].

3.7.4. Cyclic voltammetric studies. Cyclic voltammetry has also been introduced to study interaction between metal complexes and DNA, providing a useful complement to

spectral studies [53]. The binding of **1** with DNA is shown in figure 7. Cyclic voltammograms of **1** in the absence and presence of CT-DNA exhibited significant shifts in the anodic peak potentials followed by decrease in peak currents, indicating interaction between **1** and CT-DNA. The shift in the value of the formal potential ($\Delta E°$) is used to calculate the ratio of equilibrium binding constants K_{2+}/K_{3+} according to the following equation described by Bard and Carter [54],

$$\Delta E^\circ = E_b^\circ - E_f^\circ = 0.059 \log(K_{2+}/K_{3+})$$

where $E_b°$ and $E_f°$ are the formal potentials of the bound and free complexes, respectively, and K_{2+} and K_{3+} are the corresponding binding constants for the binding of reduction and oxidation species to DNA, respectively. Ratio of equilibrium binding constants K_{2+}/K_{3+} is calculated to be 3.35 that indicates strong binding of DNA with Ru(II).

3.8. *Protein (bovine serum albumin) binding experiments*

3.8.1. Absorption characteristics of BSA–Ru(II) complex. The absorption spectra of BSA in the absence and presence of **1** at different concentrations were studied (figure 8). Upon increasing the concentration of the complex, absorption of BSA increases regularly, due to adsorption of BSA on the surface of the complex. From these data, the apparent association constant (K_{app}) determined for complexes with BSA has been determined using the following equation (3) [46]:

$$1/(A_{obs} - A_0) = 1/(A_c - A_0) + 1/K_{app}(A_c - A_0)[\text{comp}] \quad (3)$$

where A_{obs} is the observed absorbance of the solution containing different concentrations of the complex at 280 nm, A_0 and A_c are the absorbances of BSA and the complex at

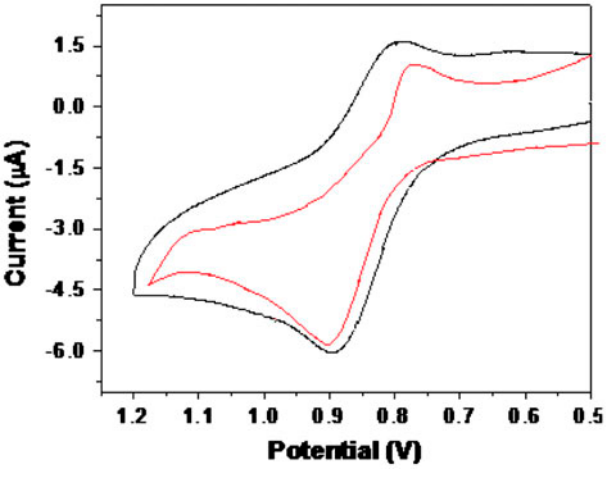

Figure 7. Cyclic voltammograms of the ruthenium(II) complex, **1** in *tris*–HCl buffer in (a) absence (black curve) and (b) presence of CT-DNA (red curve) (see http://dx.doi.org/10.1080/00958972.2013.814048 for color version).

280 nm, respectively, with a concentration of C_0, and K_{app} represents the apparent association constant. The enhancement of absorbance at 280 nm was due to absorption of the surface complex, based on the linear relationship between $1/(A_{obs} - A_0)$ *versus* reciprocal concentration of the complex with a slope equal to $1/K_{app}(A_c - A_0)$ and an intercept equal to $1/(A_c - A_0)$ (figure 8, inset). The value of the apparent association constant (K_{app}) determined from this plot is $3.7 \times 10^3\ M^{-1}$.

3.8.2. Fluorescence quenching of BSA by 1. The effect of increasing the concentration of the complex on the fluorescence emission spectrum of BSA was studied (figure 9). With the addition of **1**, BSA fluorescence emission is quenched. The fluorescence quenching is described by the Stern–Volmer relation (equation (2)). Here, I_0 and I represent the

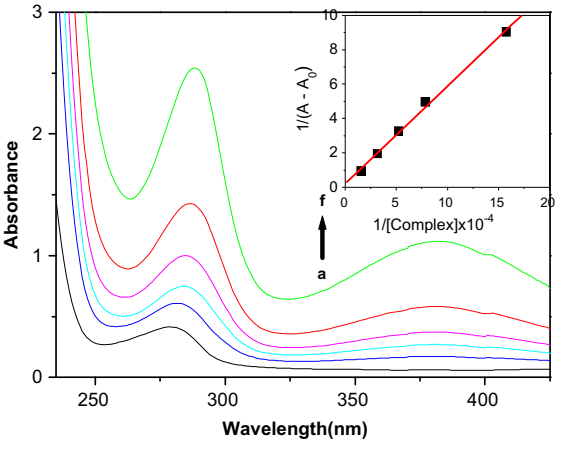

Figure 8. Absorption spectrum of BSA in the presence of complex in the concentration range $0-6.34 \times 10^{-5}$ M. Inset is the linear dependence of $1/A - A_0$ *vs*. the reciprocal concentration of complex.

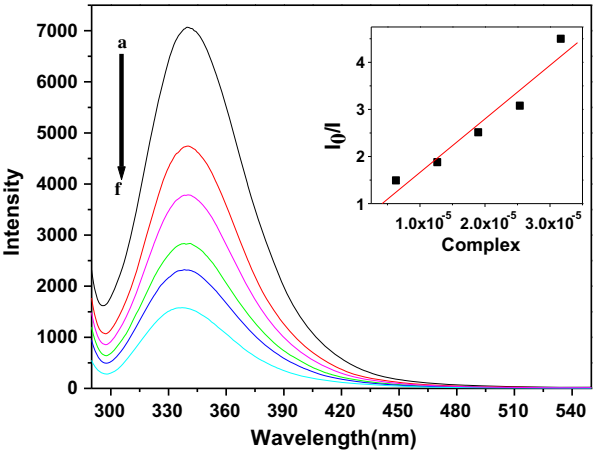

Figure 9. Fluorescence quenching of BSA at different concentrations of **1**, [complex] = 0, 1, 2, 3, 4, and $5 \times 6.35 \times 10^{-6}$ M. The inset shows the Stern–Volmer plot, the linear Stern–Volmer quenching constant (K_{SV}) $= 2.17 \times 10^5$ ($R = 0.96817$ for five points).

fluorescence intensities of BSA in the absence and presence of quencher, respectively. K_{SV} is the linear Stern–Volmer quenching constant and [complex] the molar concentration of the quencher. A linear plot (figure 9, inset) between I_0/I against [complex] was obtained and from the slope we calculated the K_{SV} as 2.17×10^5.

4. Conclusion

Synthesis and characterization of two new azopyrrole ligands, HL^1 = *(4-chloro-phenyl)-(1H-pyrrol-2-yl)-diazene* and HL^2 = *(4-nitro-phenyl)-(1H-pyrrol-2-yl)-diazene* and their corresponding ruthenium(II) complexes along with the detailed structural analysis of HL^1 by single-crystal X-ray crystallography is reported. The cytotoxicities of **1** and **2** on human cervical cancer HeLa cell line and human breast cancer epithelial cell (MCF 7 and MDA-MB 231) lines taking the Cisplatin as a positive reference clearly indicate that **1** has a higher cytotoxic acitivity against cancer cells than Cisplatin, but **2** is less active due to more electron withdrawing nitro (NO_2) group in L^2 compared to chloro in L^1 at *para* position of the azo. The spectroscopic study of interaction of **1** with CT-DNA showed groove binding, in accord with unchanged values of the viscosity of the DNA solution upon addition of **1**. This study clearly indicates that **1** binds to calf thymus DNA in a groove binding interaction [55, 56] but not in a intercalative mode like reported octahedral ruthenium(II) complexes [57–60]. However, the K_b of **1** is comparable to that of the reported ruthenium(II) complexes [55, 56]. Electrochemical studies indicate that the reduced form of the ruthenium complex (Ru(II)) has a stronger association to DNA than the oxidized Ru(III) form. Absorption and emission spectroscopy, as well as fluorescence, are used to study interactions of BSA-$[Ru(L^1)(bpy)_2]ClO_4$.

Supplementary material

Crystallographic data of HL^1 have been deposited with the Cambridge Crystallographic Data Centre, CCDC No. 885460. Copies of this information are available on request at free of charge from CCDC, 12 Union Road, Cambridge, CB21EZ, UK (Fax: +44 1223 336 033; E-mail: deposit@ccdc.ac.uk or http://www.ccdc.cam.ac.uk).

Acknowledgments

Financial support from Council of Scientific and Industrial Research (CSIR), New Delhi, India is gratefully acknowledged. A.B. and A.M. are acknowledging DBT, New Delhi for the work in cancer cells.

References

[1] W. Herbst, K. Hunger. *Industrial Organic Pigments: Production, Properties, Applications 2nd*, VCH, Weinheim (1997).
[2] A. Das, J.P. Maher, J.A. McCleverty, J.A.N. Badiola, M.D. Ward. *J. Chem. Soc., Dalton Trans.*, 681 (1993).
[3] M. Panda, S. Das, G. Mostafa, A. Castineiras, S. Goswami. *Dalton Trans.*, 1249 (2005).

[4] J. Otsuki, K. Suwa, K. Narutaki, C. Sinha, I. Yoshikawa, K. Araki. *J. Phys. Chem. A*, **109**, 8064 (2005).
[5] K.K. Sarker, D. Sardar, K. Suwa, J. Otsuki, C. Sinha. *Inorg. Chem.*, **46**, 8291 (2007).
[6] P.O. Astrand, P.S. Larsen, S. Hvilsted, P.S. Ramanujam, K.L. Bak, S. Sauer. *Chem. Phys. Lett.*, **325**, 115 (2000).
[7] R.K. Rath, M. Nethaji, A.R. Chakravarty. *J. Organomet. Chem.*, **633**, 79 (2001).
[8] S. Kannan, R. Ramesh, Y. Liu. *J. Organomet. Chem.*, **692**, 3380 (2007).
[9] J. Hannedouche, G.J. Clarkson, M. Wills. *J. Am. Chem. Soc.*, **126**, 986 (2004).
[10] J.S.M. Samec, A.H. Ell, J.B. Aberg, T. Privalov, L. Eriksson, J.E. Backvall. *J. Am. Chem. Soc.*, **128**, 14293 (2006).
[11] J.S.M. Samec, A.H. Ell, J.E. Backvall. *Chem. Commun.*, **2748**, (2004).
[12] B.K. Ghosh, A. Chakravorty. *Coord. Chem. Rev.*, **95**, 239 (1999).
[13] K.E. Erkilla, D.T. Odom, J.K. Barton. *Chem. Rev.*, **99**, 2777 (1999).
[14] H. Chen, J.A. Perkinson, S. Persons, R.A. Coxall, R.O. Gould, P.J. Sedler. *J. Am. Chem. Soc.*, **124**, 3064 (2002).
[15] A.H. Velders, H. Kooijman, A.L. Spek, J.G. Haasnoot, D. De Vos, J. Reedijk. *Inorg. Chem.*, **39**, 2966 (2000).
[16] L. Ronconi, P.J. Sadler. *Coord. Chem. Rev.*, **251**, 1633 (2007).
[17] M.J. Clarke. *Coord. Chem. Rev.*, **236**, 209 (2003).
[18] C.S. Allardyce, P.J. Dyson. *Platinum Met. Rev.*, **45**, 62 (2001).
[19] C.X. Zhang, S.J. Lippard. *Curr. Opin. Chem. Biol.*, **7**, 481 (2003).
[20] A. Hotze, M. Bacac, A.H. Velders, B. Jansen, H. Kooijman, A.L. Spek, J.G. Haasnoot, J. Reedijk. *J. Med. Chem.*, **46**, 1743 (2003).
[21] M.K. Nazeeruddin, C. Klein, P. Liska, M. Gratzel. *Coord. Chem. Rev.*, **249**, 1460 (2005).
[22] C.Y. Chen, H.C. Lu, C.G. Wu, J.G. Chen, K.C. Ho. *Adv. Funct. Mater.*, **17**, 29 (2007).
[23] A. Kukrek, D. Wang, Y. Hou, R. Zong, R. Thummel. *Inorg. Chem.*, **45**, 10131 (2006).
[24] P. Wang, C. Klein, R.H. Baker, S.M. Zakeeruddin, M. Gratzel. *J. Am. Chem. Soc.*, **127**, 808 (2005).
[25] S. Sarkar, S. Sen, S. Dey, E. Zangrando, P. Chattopadhyay. *Polyhedron*, **29**, 3157 (2010).
[26] S. Dey, S. Sarkar, H. Paul, E. Zangrando, P. Chattopadhyay. *Polyhedron*, **29**, 1583 (2010).
[27] S. Sarkar, T. Mukherjee, S. Sen, E. Zangrando, P. Chattopadhyay. *J. Mol. Struct.*, **980**, 117 (2010).
[28] A. Patra, S. Sen, S. Sarkar, E. Zangrando, P. Chattopadhyay. *J. Coord. Chem.*, **65**, 4096 (2012).
[29] R. Chakraborty, S. Chatterjee, S. Sarkar, P. Chattopadhyay. *J. Biomater. Nanobiotechnol.*, **3**, 462 (2012).
[30] B.P. Sullivan, D.J. Salmon, T.J. Meyer. *Inorg. Chem.*, **17**, 3334 (1978).
[31] CrysAlis CCD. *Oxford Diffraction Ltd (Version 1)*, Abingdon, England (2005).
[32] Z. Otwinowski, W. Minor, "Processing of X-ray Diffraction Data Collected in Oscillation Mode". In *Methods in Enzymology*, Jr. C.W. Carter, R.M. Sweet (Eds.), Vol. 276, pp. 307–309, Academic Press, New York (1997).
[33] G.M. Sheldrick. *SHELX97, Programs for Crystal Structure Analysis* (Release 97–2), University of Göttingen, Germany (1998).
[34] L.J.J. Farrugia. *Appl. Crystallogr.*, **32**, 837 (1999).
[35] C. Lee, W. Yang, R.G. Parr. *Phys. Rev. B*, **37**, 785 (1988).
[36] P. Fuentealba, H. Preuss, H. Stoll, L.V. Szentpaly. *Chemical Physics Letters*, **89**, 418 (1982).
[37] M.E. Casida, C. Jamorski, K.C. Casida, D.R. Salahub. *J. Chem. Phys.*, **108**, 4439 (1998).
[38] N.M. O'Boyle, A.L. Tenderholt, K.M. Langner. *J. Comput. Chem.*, **29**, 839 (2008).
[39] J. Marmur. *J. Mol. Biol.*, **3**, 208 (1961).
[40] M.E. Reichmann, S.A. Rice, C.A. Thomas, P.J. Doty. *J. Am. Chem. Soc.*, **76**, 3047 (1954).
[41] J.K. Barton, J.M. Goldberg, C.V. Kumar, N.J. Turro. *J. Am. Chem. Soc.*, **108**, 2081 (1986).
[42] P.K. Dhara, B. Das, J.M. Lo, P. Chattopadhyay. *Appl. Radiat. Isot.*, **62**, 729 (2005).
[43] P.K. Dhara, S. Pramanik, T.H. Lu, M.G.B. Drew, P. Chattopadhyay. *Polyhedron*, **23**, 2457 (2004).
[44] T.W. Hambley. *Coord. Chem. Rev.*, **166**, 181 (1997).
[45] H.-L. Huang, Z.-Z. Li, Z.-H. Liang, J.-H. Yao, Y.-J. Liu. *Eur. J. Med. Chem*., 46, 3282 (2011) and references therein.
[46] T.F. Chen, Y.N. Liu, W.J. Zhen, J. Liu, Y.S. Wong. *Inorg. Chem.*, **49**, 6366 (2010).
[47] R. Vijayalakshmi, M. Kanthimathi, V. Subramanian, B.U. Nair. *Biochim. Biophys. Acta*, **1475**, 157 (2000).
[48] A.M. Pyle, J.P. Rehmann, R. Meshoyrer, C.V. Kumar, N.J. Turro, J.K. Barton. *J. Am. Chem. Soc.*, **111**, 3051 (1989).
[49] L. Strekowski, D.B. Harden, R.L. Wydra, K.D. Stewart, W.D. Wilson. *J. Mol. Recognit.*, **2**, 158 (1989).
[50] O. Stern, M. Volmer. *Zeitschriff fur Physik*, **20**, 183 (1919).
[51] S. Satyanarayana, J.C. Dabrowiak, J.B. Chaires. *Biochemistry*, **31**, 9319 (1992).
[52] S. Satyanarayana, J.C. Dabrowiak, J.B. Chaires. *Biochemistry*, **32**, 2573 (1993).
[53] S. Mahadevan, M. Palaniandavar. *Inorg. Chem.*, **37**, 693 (1998).
[54] M.T. Carter, A.J. Bard. *J. Am. Chem. Soc.*, **109**, 7528 (1987).
[55] H. Paul, T. Mukherjee, M.G.B. Drew, P. Chattopadhyay. *J. Coord. Chem.*, **65**, 1289 (2012).
[56] H.-L. Huang, Z.-Z. Li, X.-Z. Wang, Z.-H. Liang, Y.-J. Liu. *J. Coord. Chem.*, **65**, 3287 (2012).

[57] C.S. Devi, S. Satyanarayana. *J. Coord. Chem.*, **65**, 474 (2012).
[58] Q.-F. Guo, S.-H. Liu, Q.-H. Liu, H.-H. Xu, J.-H. Zhao, H.-F. Wu, X.-Y. Li, J.-W. Wang. *J. Coord. Chem.*, **65**, 1781 (2012).
[59] M.N. Patel, D.S. Gandhi, P.A. Parmar, H.N. Joshi. *J. Coord. Chem.*, **65**, 1926 (2012).
[60] X.-W. Liu, Y.-D. Chen, L. Li. *J. Coord. Chem.*, **65**, 3050 (2012).